Multiyear Second Order Statistics of ALPHASAT Beacon Measurements at ASI Ground Stations

Miles Turner[1], Alef Comisso[1], Carlo Riva[1], Lorenzo Luini[1], Giuseppe Codispoti[2], Giorgia Parca[2]

[1] Department of Electronics, Information and Bioengineering (DEIB), Politecnico di Milano; Institute of Electronics, Information Engineering and Telecommunications (IEIIT), National Research Council (CNR), Milan, Italy, milesaustin.turner@polimi.it, alef.comisso@polimi.it, carlo.riva@polimi.it, lorenzo.luini@polimi.it

[2] Italian Space Agency (Agenzia Spaziale Italiana, ASI), Rome, Italy, giuseppe.codispoti@asi.it, giorgia.parca@asi.it

***Abstract*— The Alphasat Aldo Paraboni experiment by the Italian Space Agency measures signal attenuation at 19.701 GHz and 39.402 GHz using beacon signals from a geosynchronous satellite to ground stations in Tito Scalo and Spino d'Adda, Italy. Second order statistics on data collected from 2015 to 2023 are presented, supporting the understanding that higher frequencies, as seen with the 39.4 GHz beacon, are more susceptible to atmospheric fading, exhibiting higher fade percentages, steeper fade slopes, and more frequent long-duration fades. Comparisons of the measurements statistics with Rec. ITU-R P.1623-1 models show expected discrepancies, with the ITU-R models underestimating fade percentages and counts while overestimating fade slope probabilities. These findings emphasize the importance of experimental campaigns and the opportunity to further refine predictive models.**

***Index Terms*— Satellite communication, signal fading, propagation measurements, experiment.**

I. INTRODUCTION

The next generation of Satellite Communication (SatCom) systems are transitioning to utilizing higher frequency bands to meet the growing demand for larger data rates and to alleviate spectrum congestion seen in lower frequency bands such as the X, S, and K bands. Operating at these elevated frequencies offers several advantages, including increased bandwidth per service leading to higher achievable data rates, smaller hardware components such as antennas and waveguides due to the use of shorter wavelengths, and narrower antenna beamwidths enhancing beam directivity allowing for multi-beam scenarios with frequency reuse to help improve spectral efficiency [1].

However, the shift to higher frequencies such as the Ka, Q, V, and W does introduce significant challenges due to increased impairments, such as atmospheric attenuation [2]. When analyzing atmospheric attenuation, two major factors are considered: rain attenuation, which gradually increases from 10 GHz on, water vapor attenuation which will increase up until an expected peak at 22 GHz, and cloud attenuation, which is substantial at frequencies beyond 30 GHz [2]. These impairments complicate the closure of high-throughput space-Earth links, necessitating the implementation of Fade Mitigation Techniques (FMTs): indeed, relying solely on static link margins is no longer viable.

To address these challenges, comprehensive propagation experiments are essential. These experiments involve measuring signals as they traverse the atmosphere to quantify the impact of tropospheric phenomena on signal attenuation. The data collected supports the development and validation of propagation models and FMTs such as uplink power control, adaptive modulation and coding, and site diversity. This is the primary purpose of the Alphasat Aldo Paraboni propagation experiment (SCIEX), which aims to characterize impairments in the Ka and Q frequency bands [3]. Analyzing beacon measurements and deriving first and second-order statistics of the tropospheric attenuation experienced in these higher frequencies helps enhance our understanding of atmospheric effects, facilitating the accurate design of next-generation high-throughput SatCom systems. This paper focuses on the ongoing Alphasat Aldo Paraboni propagation experiment and, specifically, on the data collected for the years 2015-2023. The contribution is organized as follows: Section 2 introduces the Alphasat Aldo Paraboni propagation experiment, the total attenuation timeseries used, and how the second order statistics are calculated; Section 3 presents the results obtained when calculating second-order statistics of fade duration, fade slope, and number of fades above varying fade duration thresholds from the total attenuation timeseries. Finally, Section 4 draws conclusions that can be made from the second order statistics as well as when compared to the ITU-R models.

II. ALPHASAT ALDO PARABONI PROPAGATION EXPERIMENT

The Alphasat Aldo Paraboni experiment is an ongoing scientific campaign funded by the Italian Space Agency (Agenzia Spaziale Italiana, ASI), involving the transmission of two unmodulated continuous wave beacon signals from the Alphasat geosynchronous satellite operated by Inmarsat [3]. These beacons operate at frequencies of 19.701 GHz in the Ka-band and 39.402 GHz in the Q-band. The beacon signals are received by two Italian ground stations owned by ASI, located in Tito Scalo (southern Italy) and Spino d'Adda (northern Italy), with elevation angles of 42.1° and 35.5° and altitude heights of 765 meters and 84 meters, respectively. Each station is equipped with receiving systems that allow for a dynamic range exceeding 50 dB and a sampling rate of 16 Hz [3]. This setup enables the measurement of received power during intense rainfall events and the observation of tropospheric scintillations caused by atmospheric turbulence.

Additionally, each site is equipped with several ancillary instruments for atmospheric data collection, which assists in calculating the total site attenuation. More in detail, the sites feature a 14-channel microwave radiometer, specifically a RPG-HATPRO, which measures brightness temperatures along the propagation path to estimate slant path clear-sky attenuation levels [4]. This is a crucial measurement for accurate calibration of the received beacon signal power as further discussed in Section III. Moreover, to capture site-specific conditions, a weather station provides ancillary measurements such as air temperature, relative humidity, and atmospheric pressure, while a tipping bucket rain gauge measures the rain rate in mm/h with a 1-minute integration time.

The experiment continuously gathers time series data of the received beacon signal power at a frequency of 16 Hz, clear-sky attenuation estimates from the radiometer at a frequency of 1 Hz, and meteorological conditions, including rain rate at a frequency of 1 measurement every minute [4]. This comprehensive dataset allows for the ability to post process the data and extract the total tropospheric attenuation time series experience at both sites. By analyzing the total tropospheric attenuation time series, researchers can better understand atmospheric impairments affecting signal propagation, specifically in the Ka and Q frequency bands, supporting the development of more generalizable and accurate propagation models, and effective fade mitigation techniques when considering the use of higher frequencies.

A. Calibration Procedure

The Alphasat Aldo Paraboni experiment calculates the total tropospheric attenuation A_T from received beacon signals and additional atmospheric measurements. The beacon power level P_b measured directly from the received beacon signal includes tropospheric effects such as scintillations, atmospheric gases, clouds, and rain. The received signal P_b can be decomposed as:

$$P_b = EIRP + G_{ant} + G_{rx} - L_{fs} - A_T \quad (1)$$

where $EIRP$ is the effective isotropic radiated power, G_{ant} and G_{rx} are antenna and receiver gains, and L_{fs} is the free-space path loss. To extract the total attenuation level, A_T, a reference power level P_{ref} is used to mitigate systematic variations inherent in the first four terms [5]. The reference power level $P_{ref}(f,\theta)$ can be defined as:

$$P_{ref}(f,\theta) = P_b(f,\theta) + A_T(f,\theta) \quad (2)$$

Since A_T is still unknown, a direct calculation is not feasible. To solve this, the work in [6] adopts an approach that uses estimates of the clear-sky attenuation A_{est} using measurements from a microwave radiometer (MWR), which when combined with the received beacon power level P_b provides an estimate of the reference power level P_{ref} thus allowing the use of (2) to derive the total attenuation A_T. The MWR observes brightness temperatures at multiple frequencies sensitive to atmospheric constituents, which are then used to compute attenuation at different radiometer frequencies from the following relationship:

$$A_{ri}(f_i,\theta) = 10\log_{10}\left(\frac{T_{mr}(f_i,\theta) - T_c}{T_{mr}(f_i,\theta) - T_{sky}(f_i,\theta)}\right) \quad (3)$$

T_{mr} is the monthly mean radiating temperature, T_c is cosmic radiation, and T_{sky} is the measured brightness temperature. A linear combination of these estimates yields the clear-sky attenuation A_{est} [6]:

$$A_{est}(f,\theta) = a_0 + \sum_{i=1}^{5} a_i A_{ri}(f_i,\theta) \quad (4)$$

During rain events, the initial clear-sky attenuation and beacon power values are interpolated to obtain a new A^*_{est} and P^*_b as in [6] because the radiometer's attenuation estimates become unreliable due to multiple scattering effects in simple inversion algorithms. Using these corrected values, the total attenuation is calculated as:

$$A_T(f,\theta) = P^*_b(f,\theta) + A^*_{est}(f,\theta) - P_b(f,\theta) \quad (5)$$

To help identify rain events, the Sky Status Indicator (SSI) algorithm based on radiometer brightness temperatures presented in [7] is used, but manual inspection is also used to refine event detection.

In situations when MWR data is unavailable, Numerical Weather Products (NWP) are used to estimate the clear-sky attenuation A_{cs} based on atmospheric parameters (pressure, temperature, humidity) as in [5]. The modified calibration equation becomes:

$$A_T(f,\theta) = P'_{b,cs}(f,\theta) + A'_{cs}(f,\theta) - P_b(f,\theta) \quad (6)$$

Here, $P'_{b,cs}$ and A'_{cs} are the interpolated beacon power level and clear-sky attenuation estimate across both rain and cloud events, since A_{cs} accounts only for gaseous attenuation. This method allows for calibration of the data during radiometer outages and ensures reliable tropospheric attenuation time series for further analysis.

B. Data Preparation

After obtaining the total tropospheric attenuation time series, a thorough visual inspection of the processed data was conducted to remove any anomalies and ensure data quality [8]. Initially, automatic detection methods like the SSI were used to identify rain event windows. However, uncertainties in accurately determining the start and end times of these events necessitated additional scrutiny. Therefore, visual inspections utilizing radiometer data and ancillary weather measurements (e.g., rain rate, temperature, relative humidity) were performed to refine event identification and confirm proper calibration. This step was particularly important because the radiometer's attenuation estimates during rain events often did not coincide with those measured by the beacon receivers due to inherent inaccuracies.

Data was removed if it was deemed invalid, doubtful, or associated with system outages. Invalid data included instances where the calculated attenuation yielded unrealistic results — not attributable to tropospheric effects — such as when Q-band attenuation exceeded Ka-band attenuation or when the Sun emission affected the radiometer readings [8]. Doubtful data referred to unexpected spikes in both the beacon and rain gauge measurements that were not automatically filtered out by the software. System outages were identified during periods when the receiving station experienced operational issues. These could occur if:

1. The antenna entered 'Safe' mode (antenna locked in position), causing large variations in power levels as the beacon was picked up by the side lobes;

2. The receiver lost lock with the Ka-band beacon, evident from an instantaneous drop in beacon power.

C. Second Order Statistics

The second order statistics considered for this article are fade duration, fade slope, and the total number of fades exceeding a duration d longer than duration D for a given threshold A. The calculation of these statistics involves several steps as outlined in [9]. Fade duration is defined as the time between two crossings of the attenuation level above the threshold A. Its probability of occurrence $(d > D \mid a > A)$ is computed as:

$$P(d > D \mid a > A) = \frac{N_D}{N_A} \tag{7}$$

where N_D represent the number of fades longer than D and N_A represents the total number of fades exceeding A. The cumulative exceedance probability $F(d > D \mid a > A)$, representing the fraction of total fade time contributed by fades longer than D, is calculated as:

$$F(d > D \mid a > A) = \frac{T_D}{T_A} \tag{8}$$

where T_D represent the total fade time due to fades longer than D and T_A represents the total exceedance time of threshold A. These probabilities allow for estimating the total number of fades and the total time the threshold is exceeded over a reference period. Specifically, the total number of fades exceeding D for threshold A is found by multiplying $P(d > D \mid a > A)$ by the total number of fades $N_{tot}(A)$:

$$N(d > D, A) = N_{\text{tot}}(A)\, P(d > D \mid a > A) \tag{9}$$

Similarly, the total time during which fades of duration longer than D occur is computed by multiplying $F(d > D \mid a > A)$ by the total exceedance time $T_{tot}(A)$:

$$T(d > D, A) = T_{tot}(A)\, F(d > D \mid a > A) \tag{10}$$

For calculating fade slope, defined as the rate of change of attenuation over time, the slope ζ is obtained from filtered attenuation data to eliminate rapid variations like scintillations. The fade slope is calculated as:

$$\zeta = \frac{A(t+\Delta t) - A(t)}{\Delta t} \tag{11}$$

where $A(t)$is the attenuation at time t and Δt is the time interval

III. RESULTS

In this article, a low-pass filter with a 3 dB cut-off frequency of 0.025 Hz is used to remove scintillations, with attenuation levels of 3, 10, 15, and 25 dB, and fade slope calculated over 60 second time intervals. Table 1 presents the Ka and Q beacon signal availability for Tito and Spino from 2015 to 2023. Figures 1–6 show the cumulative exceedance probability for fade duration, fade slope, and the total number of fades exceeding threshold durations for 19.7 GHz and 39.4 GHz beacons at attenuation levels of 3, 10, 15, and 25 dB at both ground stations. Each figure also compares these measured values with the ITU-R models, calculated according to Rec. ITU-R P.1623-1, considering site-specific factors like elevation angle and beacon frequency [9].

Table I. Total availabilities of the Ka and Q beacon at Tito Scalo and Spino d'Adda for the years 2015 to 2023.

Year	**Total Beacon Availability (%)**			
	Tito Scalo		***Spino d'Adda***	
	Ka	Q	Ka	Q
2015	71.57	72.34	92.28	92.27
2016	11.71	11.07	46.42	46.41
2017	34.01	34.02	89.43	89.78
2018	37.78	37.78	54.69	54.72
2019	74.99	74.99	76.49	76.47
2020	80.39	59.17	49.94	43.88
2021	70.14	70.14	3.56	3.56
2022	71.40	71.40	57.81	57.82
2023	77.50	76.53	49.29	49.29

Analysis of fade durations (Fig. 1 and Fig. 2) reveals that the time percentage of fades decreases exponentially with increasing fade duration for both frequencies. The 39.4 GHz frequency exhibits higher fade percentages for longer durations compared to 19.7 GHz due to its greater susceptibility to atmospheric attenuation [2]. Between the two sites, Spino consistently shows higher fade percentages than Tito, especially at 39.4 GHz and larger fade durations. Notably, when comparing the ITU-R models to the measured data, the ITU-R models tend to underestimate fade percentages, especially at higher attenuation thresholds and longer durations for the 19.7 GHz beacon. However, for the 39.4 GHz beacon, the ITU-R models align well with the measured results at shorter durations but begin to overestimate fades for Tito and underestimate them for Spino as the duration increases.

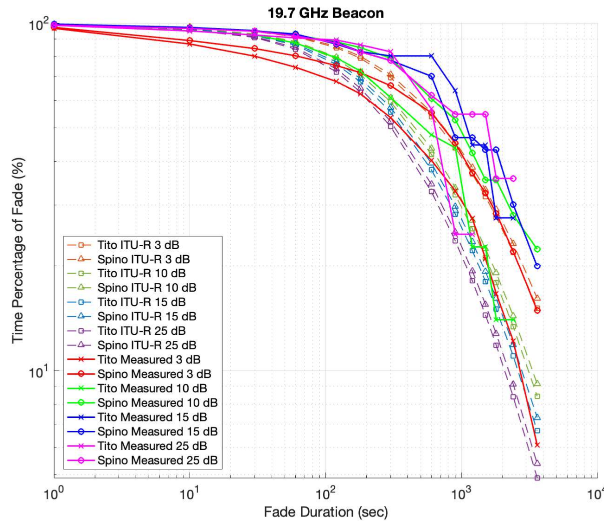

Fig. 1 Fade duration distribution for 19.7 GHz beacon signals at different fade depths.

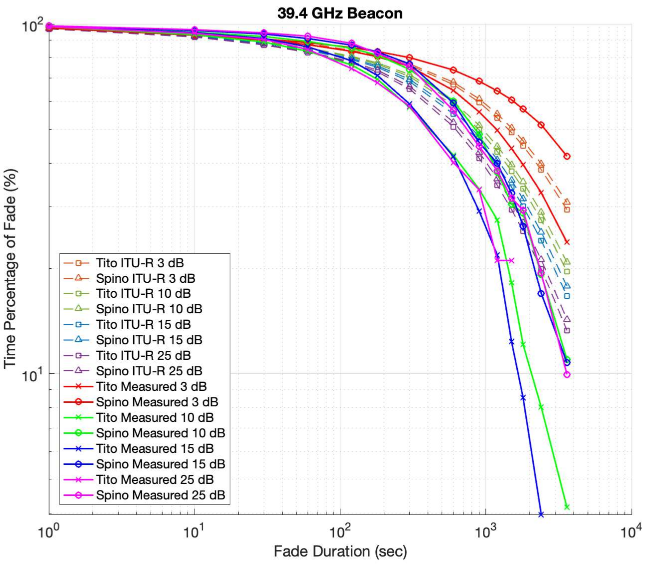

Fig. 2 Fade duration distribution for 39.4 GHz beacon signals at different fade depths.

Regarding fade slopes (Fig. 3 and Fig. 4), the probability of fade slopes slightly decreases as the fade slope (dB/s) increases for both frequencies. The 39.4 GHz beacon shows a steeper decline in probability for higher fade slopes when compared to the 19.7 GHz beacon, which is expected, as larger fade slopes are typically observed at higher frequencies for corresponding attenuation thresholds. When comparing the two sites, Spino d'Adda is found to exhibit lower probabilities of occurrence than Tito Scalo, notably at higher attenuation levels. When comparing the ITU-R models with the measured results, the former ones tend to overestimate the probability of fade slopes across all attenuation levels for both frequencies and sites.

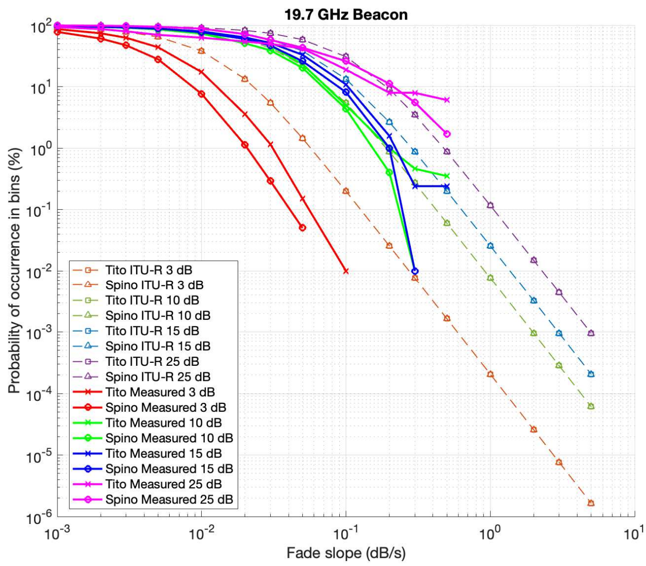

Fig. 3 Fade slope distribution for 19.7 GHz beacon signals at different fade depths.

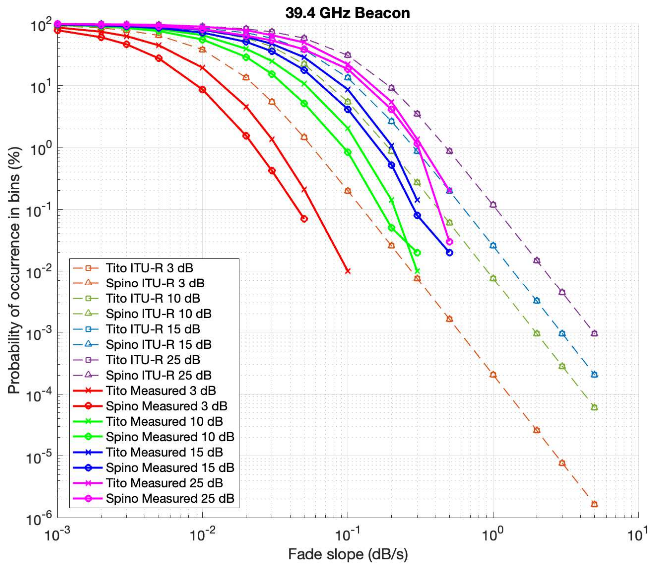

Fig. 4 Fade slope distribution for 39.4 GHz beacon signals at different fade depths.

Examining the number of fades exceeding threshold durations (Fig. 5 and Fig. 6), the data shows that the number of fades exceeding threshold durations decreases with increasing fade duration for both frequencies. The 39.4 GHz beacon generally has higher fade counts than the 19.7 GHz beacon, especially for longer durations by an order of magnitude. When considering the two sites, Spino d'Adda reports higher fade counts than Tito Scalo, at the same attenuation thresholds, and this trend seems to be more prominent at higher attenuation levels. Comparing the measured results to the ITU-R models, the latter seem to underestimate the number of fades, particularly at higher attenuation thresholds and longer durations.

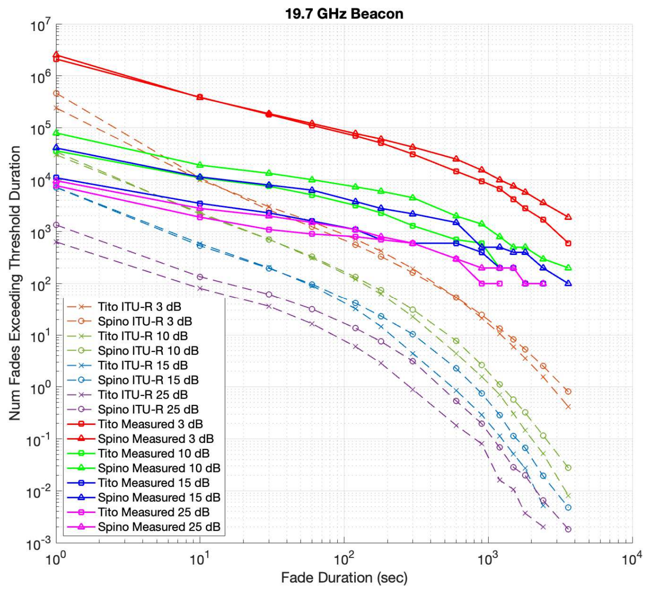

Fig. 5 Number of fades exceeding threshold duration for 19.7 GHz beacon signals at different fade depths.

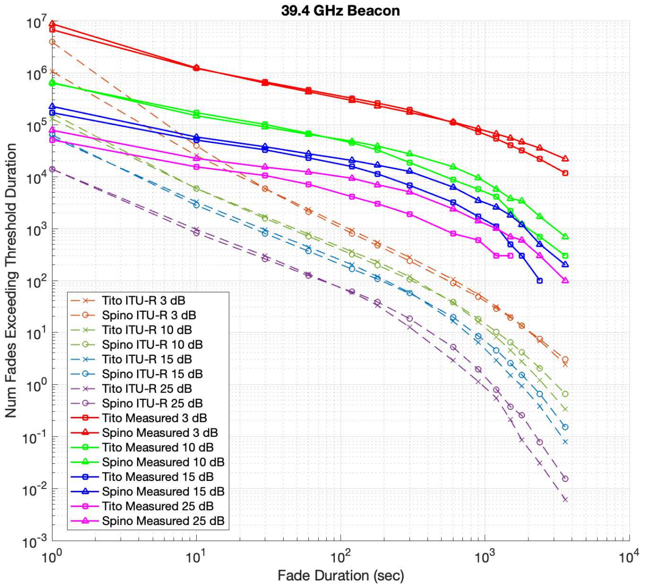

Fig. 6 Number of fades exceeding threshold duration for 39.4 GHz beacon signals at different fade depths.

IV. CONCLUSIONS

The analysis of second-order statistics for the 19.7 GHz and 39.4 GHz beacons at the Tito Scalo and Spino d'Adda ground stations reveals some notable differences between the measured data and ITU-R model predictions. The higher frequency signal at 39.4 GHz shows greater sensitivity to atmospheric attenuation, leading to higher fade percentages, steeper fade slopes, and a greater number of fades exceeding threshold durations compared to the 19.7 GHz signal. Among the two locations, Spino d'Adda experiences more severe fading effects, especially at 39.4 GHz and for longer fade durations.

Considering the ITU-R models, it can be seen that they tend to underestimate fade percentages and the number of fades at higher attenuation levels and for longer durations, while overestimating the probability of fade slopes across all levels, particularly at lower attenuation. These discrepancies, observed when comparing the ITU-R models as outlined in Rec. ITU-R P.1623-1 with the Alphasat dataset, align with expectations mentioned in [9]. Furthermore, considering the overall availability of the measured data may explain the differences between the measured data and the ITU-R models, as some of the discrepancies could be due to outages within the dataset. Similar discrepancies, within the margin of error, have also been identified in other studies comparing the same ITU-R models with measured data [10] [11].

These findings highlight the importance of the experimental campaigns and the opportunity to further refine predictive models like those included in Rec. ITU-R P.1623-1 with real-world fade behavior, especially for higher frequency communications. Accurate modeling is key to the design and reliability of satellite communication systems, and improving these models can help enhance link performance and develop better strategies for mitigating fading.

ACKNOWLEDGMENT

Authors would like to acknowledge the research project "Propagation models for future space communication systems in the Ka, Q/V and W bands in the framework of the experiment Alphasat Aldo Paraboni – ALPAKA" funded by the Italian Space Agency.

REFERENCES

[1] O. Kodheli *et al.*, "Satellite Communications in the New Space Era: A Survey and Future Challenges," in IEEE Communications Surveys & Tutorials, vol. 23, no. 1, pp. 70-109, Firstquarter 2021, doi: 10.1109/COMST.2020.3028247.

[2] ITU-R, "Attenuation by atmospheric gases and related effects", Recommendation P.676-13, Geneva, 2022

[3] T. Rossi et al., "Satellite communication and propagation experiments through the alphasat Q/V band Aldo Paraboni technology demonstration payload," in IEEE Aerospace and Electronic Systems Magazine, vol. 31, no. 3, pp. 18-27, March 2016, doi: 10.1109/MAES.2016.150220.

[4] C. Riva et al. , "The Alphasat Aldo Paraboni propagation experiment: Measurement campaign at the Italian ground stations," International Journal of Satellite Communications and Networking, vol. 37, no. 5, pp. 423-436, 2019. [Online]. Available: https://doi.org/10.1002/sat.1249.

[5] L. Luini, G. A. Siles, J. M. Riera, C. G. Riva and J. Nessel, "Methods to Estimate Gas Attenuation in Absence of a Radiometer to Support Satellite Propagation Experiments," in IEEE Transactions on Instrumentation and Measurement, vol. 69, no. 7, pp. 5116-5127, July 2020, doi: 10.1109/TIM.2019.2950612.

[6] L. Luini, C. Riva, R. Nebuloni, M. Mauri, J. Nessel and A. Fanti, "Calibration and use of microwave radiometers in multiple-site EM wave propagation experiments," 12th European Conference on Antennas and Propagation (EuCAP 2018), London, UK, 2018, pp. 1-5, doi: 10.1049/cp.2018.0906.

[7] A. V. Bosisio, E. Fionda, P. Ciotti and A. Martellucci, "A Sky Status Indicator to Detect Rain-Affected Atmospheric Thermal Emissions Observed at Ground," in IEEE Transactions on Geoscience and Remote Sensing, vol. 51, no. 9, pp. 4643-4649, Sept. 2013, doi: 10.1109/TGRS.2013.2272589.

[8] C. Riva et al., "Multiyear statistics of Alphasat beacon measurements at ASI ground stations Tito Scalo and Spino d'Adda," presented at 29th Ka and Broadband Communications Conference, Seattle, US, Sept. 2024.

[9] ITU-R, "Prediction method of fade dynamics on Earth-space paths," ITU-R Recommendation P.1623-1, Geneva 2008.

[10] D. Pimienta-del-Valle, J. M. Riera, P. Garcia-del-Pino, and G. A. Siles, "Three-year fade and inter-fade duration statistics from the Q-band Alphasat propagation experiment in Madrid," International Journal of Satellite Communications and Networking, vol. 37, no. 5, pp. 460-476, 2019. [Online]. Available: https://doi.org/10.1002/sat.1271.

[11] A. Kelmendi, A. Hrovat, A. Švigelj and M. Mohorčič, "Fade Slope Analysis of Alphasat Satellite Measurements at Ka and Q Bands," 2021 15th European Conference on Antennas and Propagation (EuCAP), Dusseldorf, Germany, 2021, pp. 1-5, doi: 10.23919/EuCAP51087.2021.9411105.